Hindawi
Shock and Vibration
Volume 2021, Article ID 9955994, 12 pages
https://doi.org/10.1155/2021/9955994

Research Article

Study on Response Characteristics of Surrounding Rock Rupture Microseismic Events during Coal Roadway Excavation

Yajuan Wang[1], **Dongji Lei**[1,2], **Yuanyuan Zheng**[1] and **Tao Ma**[1]

[1]*State Key Laboratory Cultivation Base for Gas Geology and Gas Control, Henan Polytechnic University, Jiaozuo, Henan Province 454000, China*
[2]*Collaborative Innovation Center of Central Plains Economic Region for Coalbed/Shale Gas, Jiaozuo, Henan 454000, China*

Correspondence should be addressed to Dongji Lei; leidongji@126.com

Received 25 March 2021; Accepted 7 May 2021; Published 24 May 2021

Academic Editor: chao xu; xuchaocumt@126.com

In order to solve the problems such as coal burst and abnormal gas overrun caused by the fracture of surrounding rock in the process of mining in the coal roadway, the ESG microseismic monitoring system is built on the driving face of 8005 transportation roadway of Wuyang Coal Mine to carry out a real-time, continuous, and omnidirectional dynamic state monitoring. In this way, the characteristics of time-frequency evolution and energy distribution of the acquired signals are systematically analyzed, and the location of the roadway microseismic events is studied. The results show the following: (1) influenced by mining activities, the localized microseismic events are mostly distributed in front and on both sides of the working face. Due to mining activities and geological changes, the equilibrium of original stress in coal and rock mass is broken. The stress thus is released accompanied by fracture before reaching a new equilibrium. (2) By comparing the coal and rock fracture signals with the interference signals, it is found that the fracture signals have short duration and large amplitude with obvious abrupt change characteristics. The interference signals have long duration and relatively small amplitude with less obvious change. (3) Fourier transform analysis shows that the main frequency of coal rock fracture signals is 100–200 Hz with large total energy concentrated in the first frequency band, while that of interference signals is mostly less than 100 Hz with small total energy. The research results can effectively identify the coal and rock dynamic disasters, provide technical support for the prediction and early warning of hidden danger, and guide the safe and efficient production.

1. Introduction

China is one of the countries with the largest coal output and consumption in the world. As the main energy source in China, coal plays a vital role in national economic and social development. With the increasing demand for coal resources, China's coal mining is rapidly developing to the deep areas. Underground blasting mining, excavation disturbance, and the sudden change of field geological conditions and surrounding rock characteristics can all lead to the instability of coal seam, leading to more and more serious coal and rock dynamic disasters. Coal and rock dynamic disasters have great strength and destructions. Coal and gas outburst is one of the biggest coal and rock dynamic disasters in coal mine production, which seriously threatens the safety of coal mine production [1]. Therefore, it is extremely urgent to timely predict the disasters and identify their types.

With the continuous development of information technology, successively, electromagnetic radiation method [2], acoustic emission technology [3], and microseismic monitoring technology [4] have been used to monitor coal and rock dynamic disasters, and the application of them has achieved good results. In recent years, the development of microseismic monitoring technology is particularly prominent with remarkable effects. Many scholars have carried out a lot of research and made great progress in this field. Li et al. [5, 6] studied the multifractal features and time-varying response characteristics of microseismic waveforms of the coal and rock under impact failure, based on the multifractal theory. They also expounded on the development prospect of microseismic monitoring technology. Lei et al. [7, 8]

divided mining-induced microseismic signals into blasting, coal wall caving, roof fracture, and coal wall fracture through research and analyzed the variation trend of roof fracture and coal wall fracture, which provided a basis for determining coal rock failure types. Zhu et al. [9] analyzed different types of microseismic signals by using wavelet packet five-layer multiscale decomposition and found that rock fracture signals were mostly concentrated in the $S_{5.0}$-$S_{5.7}$ low-frequency band (0–125 Hz), and blasting vibration signals were concentrated in the $S_{5.24}$-$S_{5.3}$ frequency band (375–500 Hz). This study provides a basis for further determining signal categories. Jiang et al. [10] analyzed the spectrum characteristics of different microseismic signals from the perspectives of time-domain, frequency-domain, and statistical analysis, by extracting and recognizing the waveform features of multi-channel microseismic signals of a single event. He et al. [11] studied the geological anomalies and the spatial distribution characteristics of microseismic events in the process of coal roadway excavation, with the support of microseismic frequency index, energy index, and CT detection method for vibration wave. It is found that the distribution characteristics of the regional stress field are consistent with the theoretical distribution, so a new regional dynamic monitoring method using microseismic monitoring technology is proposed for coal seam with outburst danger. With the help of the high-precision microseismic monitoring system, Zhu et al. [12] studied the space-time evolution law of microseismic events in the process of excavation and analyzed and obtained the microseismic response law of geological abnormal areas within the mining range. After analyzing the waveforms and spectrum characteristics of microseism at different energy levels, Wang et al. [13] found out waveform and spectrum characteristics under different mine earthquake intensity. Jia et al. [14] analyzed the propagation of microseismic signals in the same layer and different rock masses through laboratory tests and obtained the variation rule of the propagation velocity, frequency, amplitude, and energy of microseismic signals. Kong et al. [15] studied the dynamic development law and distribution law of microseismic events through microseismic monitoring technology. Combined with rock mechanics, mine pressure, and rock seam movement theory, they deduced the roof rock seam movement law of fully mechanized caving faces of extrathick coal seam. Guo and Dou [16] analyzed the plane distribution of microseism, variation law of energy and frequency with working face advance, and waveform characteristics of microseismic signals in fault areas. It is found that the elastic stick-slip vibration process of surrounding rock is the most important stage of energy release, the vibration generated in the plastic stick-slip failure process of surrounding rock is low in frequency and energy, and the microseismic signals are characterized by long duration, low frequency, small amplitude, and slow attenuation. Yang et al. [17] combined microseismic monitoring means with field measurement, numerical simulation, and theoretical analysis to conduct a rockburst monitoring study on No. 705 working face of Baojishan Coal Mine and found that dynamic load is an important cause of rockburst. The rockburst prevention technology combining anchor mesh and cable support with high-pressure water jet unloading is put forward, which provides a theoretical basis and new guidance for the synergistic effect of roadway to prevent rockburst. Conducting microseismic monitoring in No. 117 mining area of Dongteng Coal Mine, Ren et al. [18] successfully analyzed and found the difference in time-frequency characteristics and propagation distance between interference signals and coal fracture signals and proposed that the on-site interference signals could be removed by the corresponding algorithm. Through field measurement and theoretical analysis, Yang et al. [19] revealed that the cause of rockburst in a soft coal seam is mainly caused by a disturbance zone formed under the high stress, which makes the coal seam unstable. In view of this, they proposed prevention and control measures ranging from identifying potential impact area and synchronously monitoring coal stress and roadway deformation to implementing preventive measures. Wang and Zhu et al. [20] used SOS microseismic monitoring system to monitor and collect microseismic events and data in the mining process of multiple coal seams and systematically analyzed the characteristics and differences of microseismic events in the mining process of multiple coal seams under high thick and hard rock seam. This study revealed the spatial-temporal evolution characteristics of microseismic events and the mechanism of rockburst induced by high thick and hard rock strata is discussed. The instantaneous variability of dynamic failure of mine surrounding rock made it difficult to capture signals. In addition, the interference of external conditions and the low sensitivity of sensors caused the miss of many signals which are supposed to be effective, thus the monitoring effect was not as valid as it should have been.

Most of the research on mine burst damage by the above microseismic monitoring technology is carried out on the platform such as numerical simulation, having little connection with the field production. Therefore, the analysis lacks reliability and practical value. Considering that the actual monitoring should be carried out according to the mine production activities, this paper takes the mining face of 8005 transportation roadway of Wuyang Coal Mine as the test background. Aiming at the phenomenon of repeatedly loud coal bursts in the mine, a comprehensive, real-time, and continuous underground microseismic monitoring system is constructed by using a high-sensitivity uniaxial acceleration sensor. The field driving work records are summarized to extract the effective signal characteristics. And select typical events for gas, geology, and microseismic analysis to judge the occurrence regularity of coal rock fracture microseismic, so as to provide a theoretical basis for the prevention of coal rock dynamic disasters.

2. The Geological Survey of the Test Working Face and the Arrangement of Microseismic Monitoring System

2.1. Geological Conditions of the Test Working Face. Wuyang Coal Mine is located in the Nanfeng exploration area of Lu'an mining area in Qinshui coalfield. At present, five main development roadways are arranged along the axis

of the Tianchang syncline. The test working face belongs to 8005 transport roadway in 3# coal seam, which is close to the 8006 working face on the south and near the axis of the east anticline. Its stress surface is mainly squeezed by the roof. In the process of excavation, some areas of the coal seams are affected by faults, and there are small faults such as S104 and S105, syncline S1, and other tectonic influenced areas, which can easily form periodic pressure resulting in fluctuation. The geological structure diagram of the test working face is shown in Figure 1. With the advance of the working face, the original stress equilibrium in the coal and rock mass is broken, and the compression caused by the fault activity produces transpression and compression on the coal. The shift of abutment pressure distribution of overburden seams in roadway leads to frequent coal rock activities in roadway, which can easily lead to coal rock dynamic events. Table 1 shows the gas geological parameters of 3# coal seam.

2.2. Design of Microseismic Monitoring Scheme. The microseismic monitoring system is composed of two parts: the main engine system outside the well and the downhole data acquisition system. Among them, the data acquisition system is laid out in 8005 transportation roadway, with a total of six data acquisition channels. The collected data are transmitted to the ground in real time through an optical cable. The sampling frequency of the whole monitoring system is set as 10 MHz, and its threshold value is set as 80 mV. The uniaxial sensor used is Nano30 type (parameters are shown in Table 2), which is arranged in the coal seam and rock roof of the roadway. Sen1–Sen6 are arranged in two oblique fan shape sections according to the sequence number. As shown in Figure 2, the specific locations of the six sensors are laid out. Sen1, Sen3, and Sen5 are laid at the middle of the centerline of the roof. Sen2 and Sen6 are laid on the right side of the roadway at the mining face with a height of 1.5 meters. Sen4 is located on the opposite side of the stopping face (outer side) with a height of 1.5 meters. Among them, Sen1 is installed at the front end and the absolute distance from the heading head is 70 m. The downhole data acquisition system, Paladin system, uses 24-bit analog-to-digital conversion and sampling rates range from 15 Hz to 10 kHz.

Microseismic monitoring technology is a geophysical real-time monitoring technology which studies and evaluates the stability of coal and rock mass by using the vibration wave signal generated during the process of coal rock fracture under load [21, 22]. Based on the ESG system laid in 8005 transport roadway, this paper studies the coal rock fracture activity at 50~200 m in front of the heading face in March 2020 and the microseismic activity law of surrounding rock under the excavation of the heading face. Through microseismic monitoring, the characteristics and distribution rules of different coal and rock dynamic disaster signals are effectively analyzed, and the stability of coal body internal structure is evaluated, which provides theoretical support for coal and rock dynamic disaster prevention in underground operation.

3. Temporal and Spatial Evolution of Microseismic Events at Experimental Working Face

Spatial response is a kind of technology to locate the microseismic events using waveform identification and spectrum analysis methods. It can extract the effective microseismic wave shape after the artificial filtering of various interference signals in the mine. As shown in Figure 3, the microseismic monitoring range in deep mining of coal roadway is large, mainly focusing on the microseismic events during the mining period of 50~200 m ahead along roadway. At present, the mining depth of Wuyang Coal Mine has reached more than 700 meters. Under the influence of excavation work, the internal instability of coal and rock mass led the stress to redistribute, and the dynamic events of coal and rock are caused by the dislocation of upper and footer walls of faults near the roadway. With the continuous advancement of the mining work, microseismic events of different energy levels occurred successively in 8005 transportation roadway in March 2020, and at the same time, a large coal rock rupture event (event shown in light blue in the figure) occurred in front of the mining working face. As calculated by wavelet packet, there are 394 small seismic events with energy below $9.98E+06$J, accounting for about 50.2% of the total number of March; there are 314 of them with energy between $1.00E+07J$ and $9.93E+08J$, accounting for about 40%; and there are only 77 of them with energy above $1.05E+09J$, accounting for 9.8%. It shows that the driving face of 8005 transportation roadway is dominated by small and medium energy microseismic events, so it can be judged that the impact risk of driving face is small.

According to statistics, among the 785 microseismic events that occurred in March, the low-energy events were the majority, mainly distributed in the 50–100 m area in front of the roadway in the fault active area, and a few on both sides of the roadway. It was mainly due to the fact that the acceleration of excavation speed resulted in the working face advancing constantly towards the geological structure area, to meet the required schedule slowed down by the previous excavation work stoppage. The stress concentration was formed by the superposition of advanced support pressure and fault stress. The stress of coal and rock mass under the influence of disturbance was greater than the strength limit, which led to the instability of coal and rock mass. Therefore, the coal and rock in front of them broke and collapsed. After that, the roof support force was transferred to the coal walls on both sides of the roadway and the staggered position of the rear roadway. Suffering the stress instability, the coal body entered into an adjustment stage. The reequilibrium of internal stress distribution was often accompanied by microfracture.

According to the requirements of the mine owner, the tunneling requirement of 8005 transport roadway was 8 m/day. Upon verification, we knew that the roadway tunneling speed basically met the requirements before March 10, and on the 11th, the tunneling schedule was slightly behind. In order to ensure safe production, the miner adopted

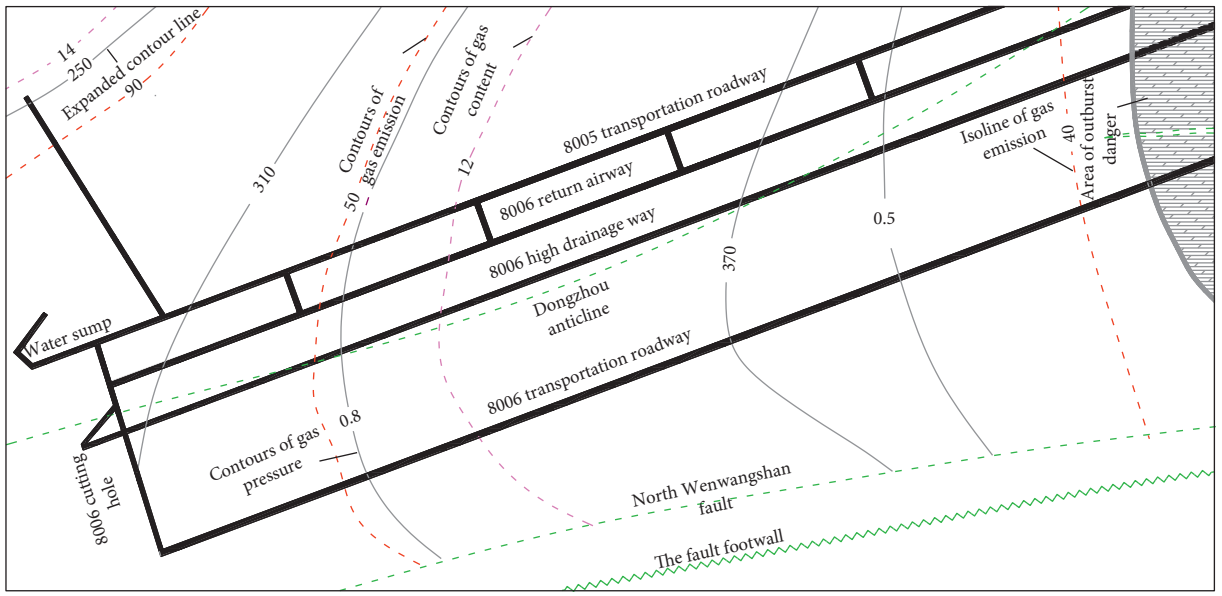

Figure 1: Geological structure map of test working face.

Table 1: 3# geological parameters of gas in 3# coal seam.

Coal seam	Mean thickness	Dip angle	Firmness coefficient	Initial seep of diffusion	Gas pressure
3#	5.54	4~14	0.23~0.89	10.5~16	0.72

Table 2: Sensor layout parameters.

Sensor number	Sen1	Sen2	Sen3	Sen4	Sen5	Sen6
Location of sensors	Centerline of the roof	The right side of the roadway	Centerline of the roof	Opposite side of the stopping face	Centerline of the roof	The right side of the roadway
Height (m)	/	1.5	/	1.5	/	1.5
Drilling depth (m)	2.5	2.5	2.5	2.5	2.5	2.5
Distance from the heading head (m)	70	110	150	190	230	270
Frequency range (Hz)	125–750	125–750	125–750	125–750	125–750	125–750

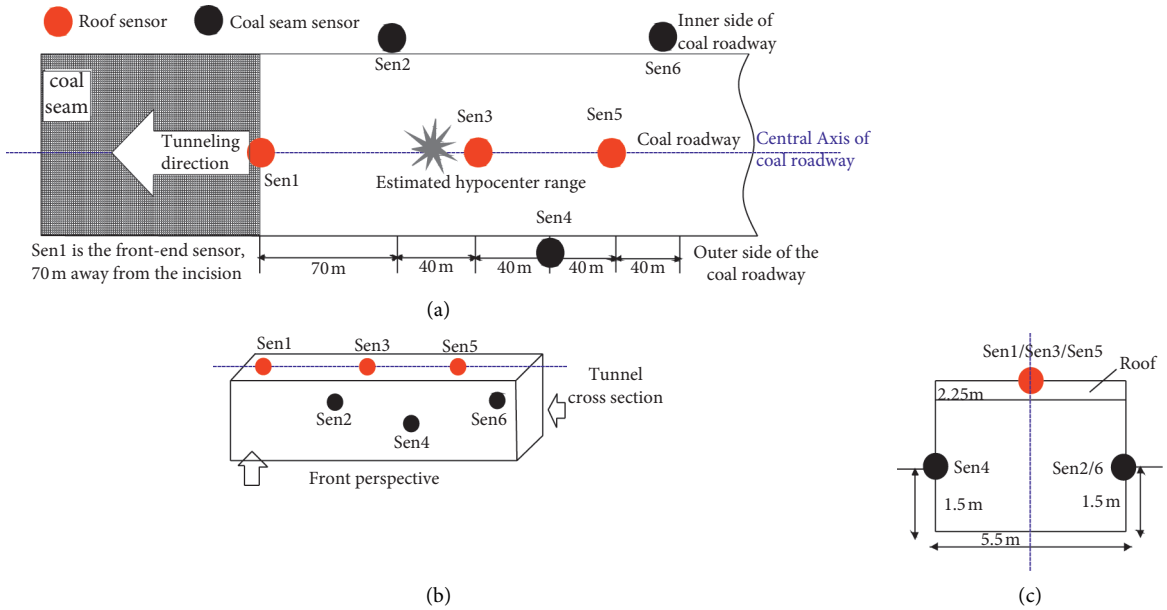

Figure 2: Three views of sensor layout in 8005 Haulage roadway. (a) Layout diagram of roadway trend sensor. (b) Front perspective of roadway sensor layout. (c) Roadway sectional view.

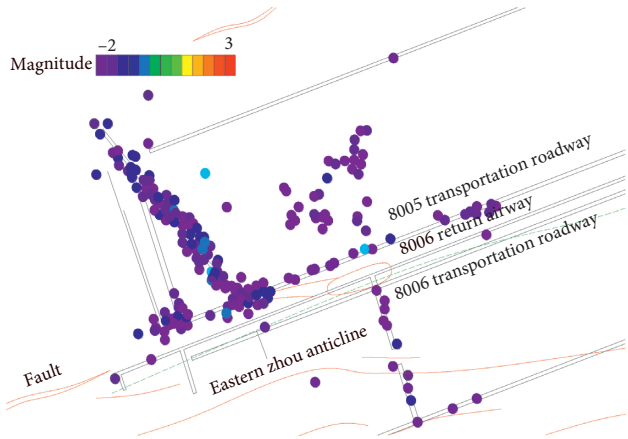

Figure 3: Distribution plan of microseismic events induced by roadway tunneling.

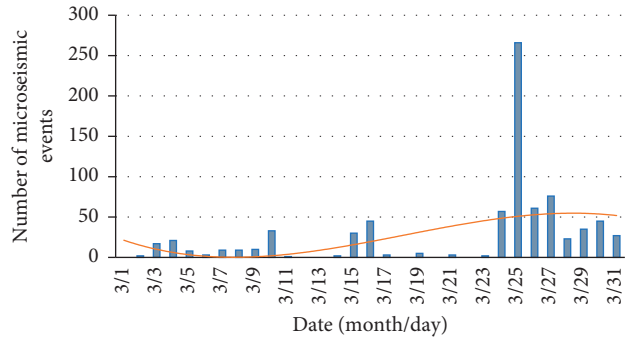

Figure 4: Daily statistical trend of microseismic events in March.

hydraulic punching cavitation and other coal seam pressure relief measures. From March 12 to 13, the roadway was not constructed and was in a stable state as a whole, and no microfracture phenomenon of coal and rock was found. Compared with the previous period, the number of microseismic events detected decreased significantly, and the energy also decreased accordingly. After pressure relief, the tunneling speed resumed. It indicates that the number of microseismic events increases with the acceleration of tunneling speed and conversely decreases. It can be seen from this that the frequency and energy release of microseismic signals near tunneling face are closely related to the working procedure of roadway.

In order to more clearly analyze the distribution rule of microseismic events in the process of tunneling, the statistical period was reduced. As shown in Figure 4, the number of microseismic events in March was counted. As can be seen from Figure 4, more than 60 microseismic events occurred from March 1 to 7, most of which were concentrated at the inflection point and on both sides of the tunneling roadway. Two microseismic events with large energy levels occurred in front of the working face, indicating that there was stress concentration of coal and rock mass and intense stress release caused by excavating work in this area. From March 8 to 14, a total of 55 microseismic events occurred, and the energy levels of the microseismic events were all small, which were caused by the small coal falling due to the excavation disturbance and the collision of working objects. A total of 86 microseismic events occurred from March 15 to 22, which increased significantly compared with the previous two weeks. However, most of them were medium- and low-energy microseismic events, which would not cause harm to the excavation work. A total of 566 microseismic events occurred from March 23 to 31, and the number of microseismic events increased significantly. The number of microseismic events increased sharply on March 25, reaching more than 260 per day. As the heading advances, the disturbance influence range also moved forward, and most microseismic events were concentrated in front of the heading face and on both sides of the roadway, of which the single frequency of microseismic events with the maximum magnitude reached 232 Hz and the energy reached $1.19E+10J$. After verification, the excavation was proceeding to an area of active geological structure at the time of this large energy event, showing that when tunneling is carried out near the geological structure zone, the intensity and energy frequency of coal and rock dynamic accidents induced by the superposition of coal body dynamic and static loads were greater. At this time, it was necessary to pay close attention to the geological structure around the roadway to further study and analyze the cause of the accident and take timely pressure relief measures [23].

4. Analysis of Time-Frequency Characteristics of Microseismic Events in Coal Roadway Tunneling

Time-frequency analysis is one of the main methods of seismic signal analysis, and it is an effective method to describe the nonstationary characteristics of digital seismic waves [10]. The dynamic failure of surrounding rock releases energy in the form of shock wave and then transmits it to the sensor. Through the microseismic wave shape, the duration from the initial arrival of the signal to the recovery of stability as well as the strength of the microseismic signal and other pieces of information can be intuitively seen [6].

4.1. Analysis of Time-Domain Characteristics of Surrounding Rock Dynamic Microseismic Signals. Time-domain analysis can directly observe the shape characteristics of the signals and effectively identify the dynamic events of surrounding rock corresponding to the microseismic signals. In Table 3, statistics of the number and orientation of sounding coal bursts in 8005 roadway are presented. As can be seen from Table 3, in the first half of March, there were a lot of noisy coal cannon incidents, and the noise location was mainly distributed in front of the working face and on the roadway roof, while it obviously decreased in the second half of March. This is mainly due to the fact that while the tunneling work was arriving near the upper and footwall of the fault in the early part of March and the roadway was extremely unstable under the influence of disturbance, there were a large number of loud coal guns. After the hydraulic cavitation and gas phase fracturing were adopted to remove the

Table 3: Statistics of roadway coal burst.

Date	Number	Location	Frequent period	Number
March 1 to 7	152	In front of the working face	March 4, 4 : 11–5 : 46	12
			March 5, 9 : 22–10 : 50	14
			March 10, 22 : 26–23 : 25	16
March 8 to 14	200	In lateral front of the working face	March 10, 1 : 35–4 : 00	14
			March 11, 18 : 43–19 : 34	12
March 15 to 22	65	On one side of the roadway		
March 23 to 31	84	In front of the working face and on the roof		

danger, the sound of loud coal bursts decreased significantly in the late part of March.

Studies show that coal and rock dynamic disasters often occur in the axis of anticlines and synclines, especially near faults and in dip angle change zones, coal seam folding, and tectonic stress zones [24]. Coupling of coal and rock dynamic disasters with gas geological structure will occur when the gas pressure, in situ stress, and coal and roof strength are within a certain range [25]. 8005 transport roadway is located in an active fault zone with a 4–14°coal seam dip angle. The tunneling face, where the geological structure is complex, is close to the Eastern Zhou anticline. The increase of fault shear stress and decrease of normal stress caused by mining activities may induce mine seismic activity. With the continuous advancement of tunneling work, the roof activity is more and more intense. On March 23–30, the coal seams are extremely unstable. There are continuous loud coal bursts and large coal dust in the mine. Strong coal and rock dynamic phenomenon signals are selected, and their amplitude and total energy are calculated by fast Fourier transform and wavelet packet algorithm. As shown in Figure 5, the microseismic waveform can directly see the intensity change of the signal during the period from the initial sensor to the stable recovery.

Large-scale rock rupture occurred in the roadway tunneling on March 23 and 24, and the hypocenter was located at $X = 4036476$, $Y = 406152$, and $Z = 83.48$. After analyzing the data collected during this period, it can be seen from Figures 5(a) and 5(b) that the rock rupture signals are short and rapid, with short duration and large amplitude, and have reached the highest amplitude acceptable to the sensor (4096 mv). Their coda waves are prominent. The total energy calculated by the wavelet packet energy algorithm is $3.4–3.9e + 09J$, and the energy is mainly concentrated in the first frequency band, the low-frequency band, indicating that the stress field of the surrounding rock is caused by the comprehensive influence of fault and underground excavation disturbance. As the tunneling work continued to advance to the fault, the fault was activated, and the peak value of the leading stress at each fulcrum of the roadway increased continuously and reached the maximum value when the tunneling work reached the fault line [19]. Two dull coal bursts were recorded on March 28 and 30. The specific time recorded by the ESG system was 8 : 28 : 31 on March 28 and 14 : 50 : 35 on March 30, when coal caving appeared in front of the heading roadway, and the hypocenters were $X = 4036310$, $Y = 406256$, and $Z = 495.51$ and $X = 4036505$, $Y = 406096$, and $Z = 684.71$, respectively. As can be seen from Figures 5(c) and 5(d), the coal collapse signal waveform lasts for a long time. The amplitude of the initial sensor of the signal has reached 4096 mV and will last about 10 ms; the amplitude of the later period decreased and returned to stability. The total energy calculated by the wavelet packet is $8.9–9.9E + 09J$, concentrated in the first band. By analyzing the time-frequency and time-domain characteristics of signals and verifying the coal and rock fracture types with field records, it is found that the gas content and gas pressure increase when the coal and rock dynamic phenomenon occurs, and the highest gas content has reached 28 m^3/t. The coal and rock fractured gas is released, and the gas content and gas pressure of coal body decrease accordingly. To classify coal and rock dynamic phenomenon signals and interference signals, the downhole interference signals and type 2 signals were selected for comparison and analysis. As shown in Figure 5(e), the interference signal waveform is relatively scattered, and the wavelet packet energy is low, only $1.2–1.4e + 04J$. Coda wave is not prominent. According to the audio extraction and identification of the data, it is found that most of them are from the underground workers' operation, mechanical operation, and object collision.

4.2. Analysis of Frequency-Domain Characteristics of Surrounding Rock Dynamic Microseismic Signals. The components of microseismic signals collected during mining are relatively complex, and it is not possible to obtain their internal characteristic information by time-domain analysis alone [26]. Therefore, in this paper, frequency-domain analysis is added on the basis of time-domain analysis to further reveal the response characteristics of coal rock fracture signals. At the same time, S-transform frequency-domain analysis is carried out on the basis of Fourier transform. The details are as follows.

4.2.1. Short-Time Fourier Transform of Microseismic Signals. The short-time Fourier transform (STFT) is derived from the classical Fourier transform, on which the time-window function is added. STFT overcomes the interference of cross term in nonstationary signal analysis and is a powerful tool for nonstationary signal analysis. Its function expression can be as follows, where $t = t'$:

$$\mathrm{STFT}(t', f) = \int_{-\infty}^{\infty} h(t) g(t - t') e^{-2j\pi f t}\, dt\,. \quad (1)$$

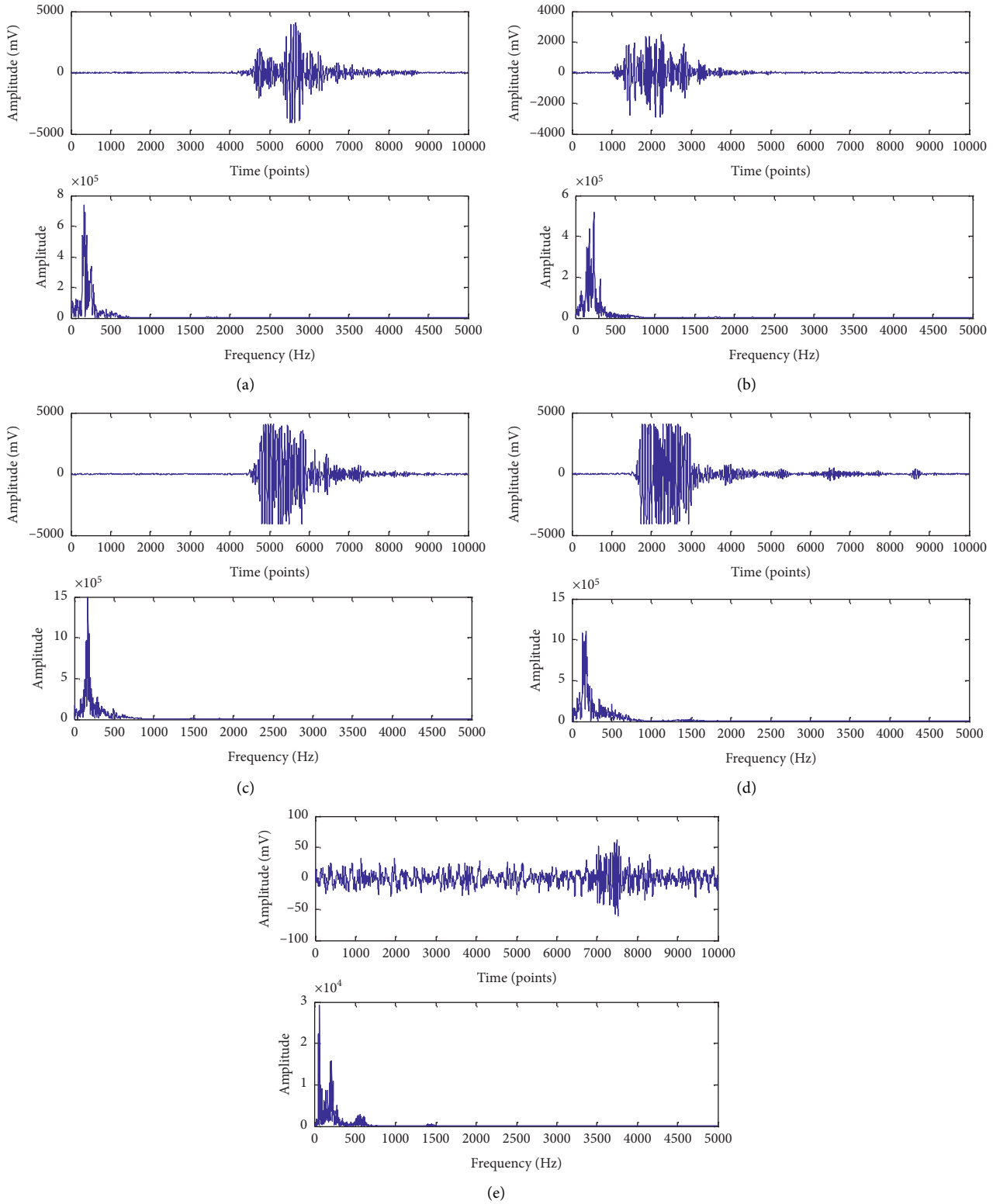

FIGURE 5: Signal waveform extraction of different microseismic events: (a) rock fracture signal, (b) rock fracture signal, (c) coal caving signal, (d) coal caving signal, and (e) noise signal.

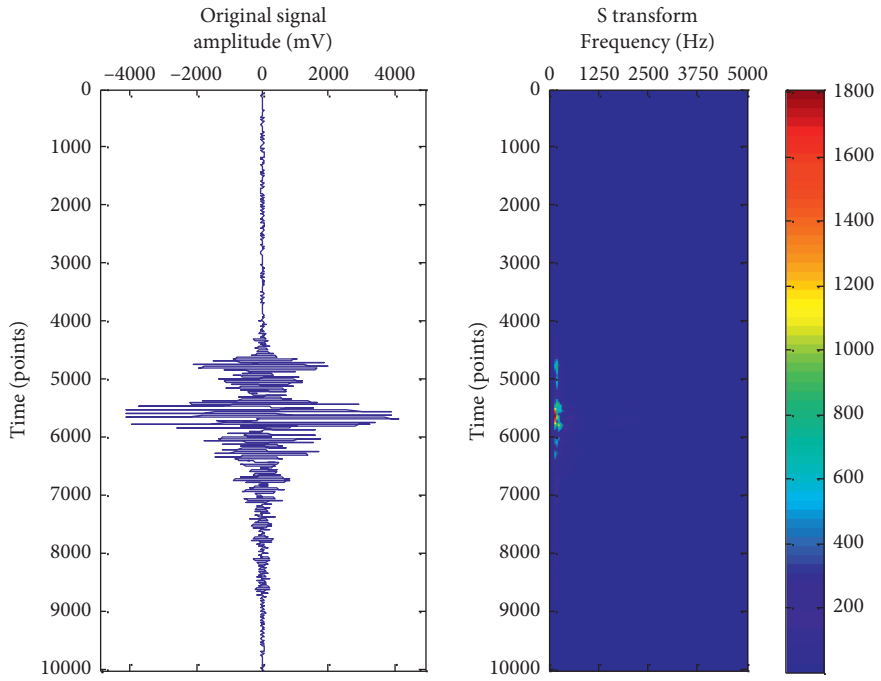

(a)

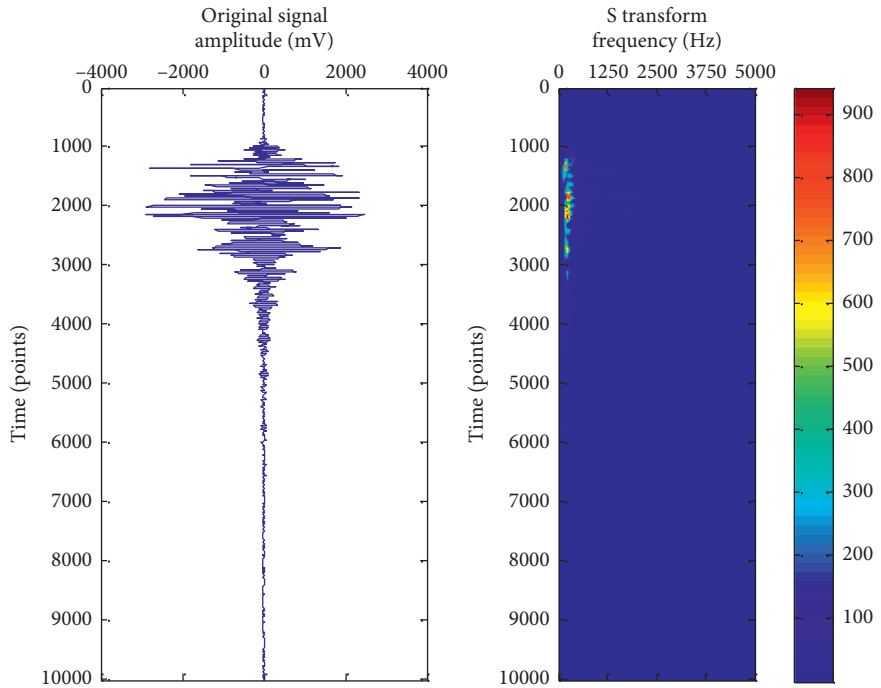

(b)

Figure 6: Continued.

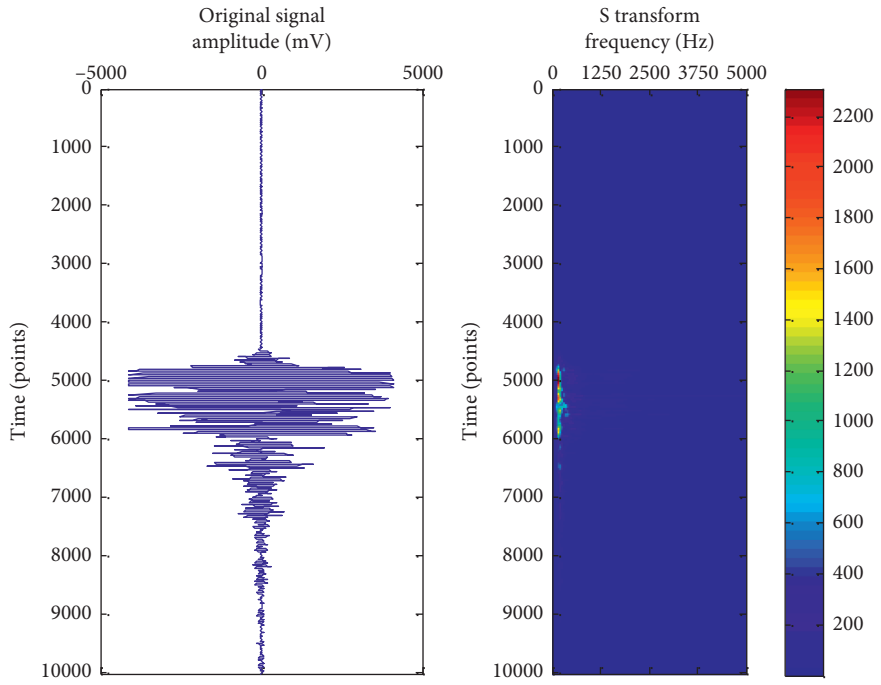

(c)

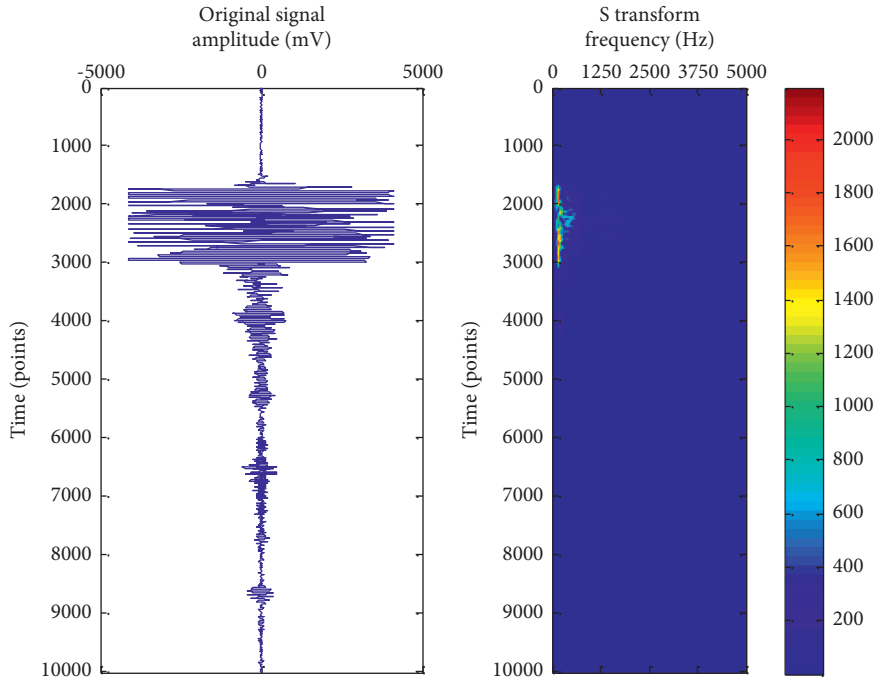

(d)

Figure 6: Continued.

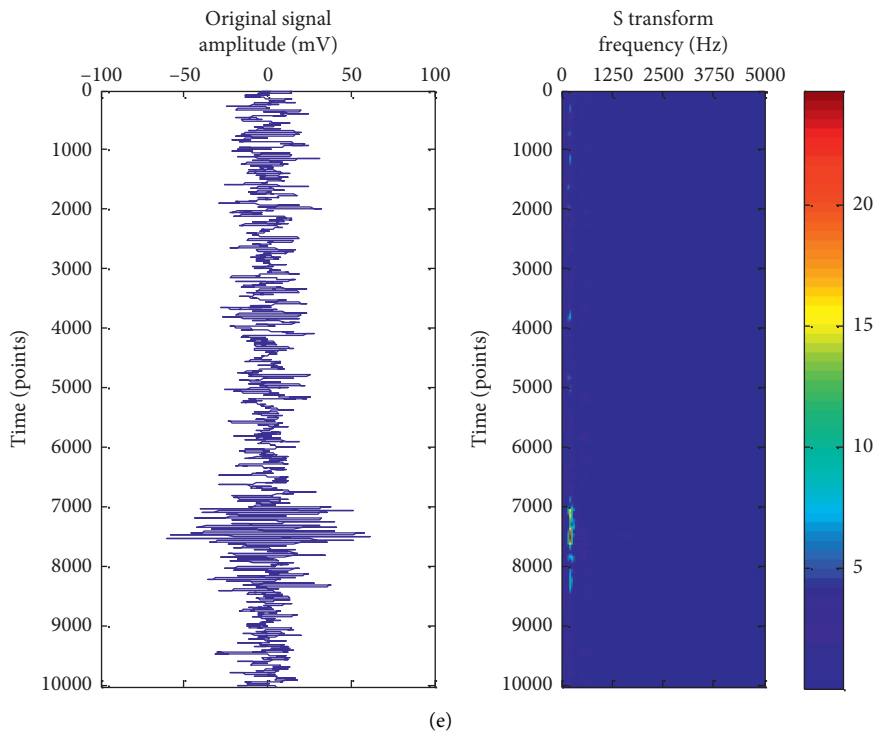

Figure 6: Comparison of S-transform results of different microseismic events. (a) S-transform cloud map of rock. (b) S-transform cloud map of rock. (c) S-transform cloud map of coal fracture caving. (d) S-transform cloud map of coal caving. (e) S-transform cloud map of noise signal.

In the formula, f denotes frequency; $h(t)$ denotes analyzed signal; $g(t)$ denotes window function; t denotes time.

4.2.2. Frequency-Domain Analysis of Microseismic Signal S-Transform. S-transform adds a time-frequency window that can be adjusted with the change of signal characteristics, so it can further analyze the frequency-domain components of the signal and accurately find out the dominant frequency contribution point, which is suitable for the analysis of nonstationary signals. By adding Gaussian window function on the basis of STFT, the S-transform corresponding to the time-window width and the frequency of the analysis signal can be obtained.

By substituting the Gaussian window function $g(t) = 1/\sqrt{2\pi}\delta e^{-(t^2/2\pi^2)}$ into the STFT expression, the following results can be obtained [26]:

$$STFT'(\delta, t, f) = \int_{-\infty}^{\infty} h(t) \frac{1}{\sqrt{2\pi}\delta} e^{-\left((t-t')^2/2\delta^2\right)} e^{-2j\pi f t} dt \,, \tag{2}$$

wherein, by substituting $\delta(f) = 1/|f|$ into equation (2), we can get [26]

$$S(t, f) = \int_{-\infty}^{\infty} h(t) \left[\frac{|f|}{\sqrt{2\pi}} \exp \frac{-f^2 (t' - t)^2}{2} \cdot \exp(-2j\pi f t) \right] dt \,. \tag{3}$$

The S-transform results of the three signals are shown in Figure 6. It can be seen that the frequency of coal caving and rock fracture signals is relatively concentrated, while that of noise signals is relatively dispersed. The two rock mass fractures in the roadway on March 23 and 24 were accompanied by small rock fracture and caving events. The main frequency of rock fracture was about 170 Hz, and the frequency of small rock fracture and caving events ranged from 0 to 80 Hz. Through S transformation, it can be seen that after the rock mass fracture in the roadway, the supporting force dropped greatly and the pressure was transferred to the coal body rapidly. The coal caving events that occurred on March 28 and 30 were composed of large-scale coal collapse and small coal fall events. Its coda wake of this signal is obviously developed, and the main frequency of the event is 160–180 Hz. Combined with Figures 5(c) and 5(d), it can be seen that coal caving lasts for a long time, so it will have a great impact on roadway operations. However, small coal caving events occur in a small range with low intensity and frequency of 50–60 Hz, which will not have a great impact on well work. Compared with rock fracture and coal caving events, the frequency of noise interference signals is the lowest, which is 30–60 Hz, and the signals are intermittent, mainly from downhole mechanical operation or slight impact of objects.

As can be seen from Table 4, the time-domain characteristics of coal caving and rock fracture microseismic signals caused by tunneling are far greater than noise interference signals in terms of occurrence time and amplitude, and so are the frequency-domain characteristics in terms of wavelet packet energy and signal main frequency. According to this result, the types of microseismic events can

Table 4: Time-frequency characteristics of different microseismic events.

Event category	Event	Time-frequency characteristics			
		Duration L (ms)	Maximum amplitude A (mV)	The total energy of the wavelet packet	Dominant frequency f (Hz)
Noise interference	Event 1	613	61.69	$3.5136e+09$	57
Coal caving	Event 1	3104	4096	$8.7179e+09$	171
	Event 2	3074	4096	$9.9744e+09$	232
Rock fracture	Event 1	3494	4096	$1.2611e+06$	166
	Event 2	2190	4086	$1.4596e+06$	167

be identified and the mine side can be guided for safe production.

5. Results and Discussion

Taking 8005 transportation roadway of Wuyang Coal Mine as the test background, the whole process of microseismic monitoring was carried out by connecting gas, geology, and microseism. The microseismic events that occurred in the tunneling work were statistically analyzed in this paper. By comparing the time-frequency characteristics of the three types of microseismic events including coal caving, rock rupture, and interference signals, we can see clearly the frequency-domain situation of each part of the signal and the overall frequency component of the signal. Further analysis and determination of the high- and low-frequency boundaries of various signals and the source of signal main frequency components show that, in the process of coal failure and rock failure, the internal stress of coal rock will transfer from the fracture point to the periphery, but the failure intensity will be greatly reduced. It can be seen that the amplitude, frequency, and energy of microseismic event signals obey coal caving signals > rock failure signals > noise interference signals. The amplitude of coal caving and rock fracture intensity has reached 4096 mV, which is maximum amplitude that the sensor can receive, while the amplitude of noise interference signals is much smaller, only about 60 mV. It can be seen that the coal and rock dynamic phenomenon caused by the geological structure has a serious impact on mine production, so it is particularly important for the microseismic monitoring technology to carry out timely early warning.

6. Conclusion

(1) According to the analysis of spatial evolution characteristics of microseismic events in the process of No. 8005 transportation roadway excavation, the microseismic events are mostly distributed near faults, in front of the working face, and on both sides of the roadway. Under the influence of mining activities, the internal stress of coal and rock mass was destroyed; then a new equilibrium state was found later. In this process, the upper and footwall of the fault dislocation lead to coal rock fracture events, and the number of microseismic events has a linear relationship with the tunneling speed.

(2) By comparing and analyzing two types of typical microseismic events (coal caving and rock mass rupture) with noise interference events, it is found that the main frequency of coal caving signal is 160–180 Hz, the main frequency of rock fracture signal is 170 Hz, and the main frequency of noise signal is 30–60 Hz. The coal caving signal and rock fracture signal are continuous, and multiple groups of signals are similar, featuring rapid attenuation, short duration, high frequency, and high specific gravity.

(3) According to the wavelet packet calculation of frequency band energy, the energy distribution of all kinds of signals is consistent, concentrated in the first frequency band. The total energy of noise interference has no obvious distribution range. The time-frequency characteristics of the three kinds of signals are all in accordance with coal collapse > rock mass fracture > noise interference.

(4) Both the duration and released energy of the two kinds of microseismic signals, coal caving and rock rupture, are relatively large, indicating that the impact caused by the two kinds of microseismic events will cause a sudden increase in the deformation energy of the surrounding rock of mine roadway, leading to large-scale failure events and changes in the distribution of the internal stress field of coal and rock mass, accompanied by the increase of gas content and gas pressure.

Data Availability

The data supporting the conclusion of the article are shown in the relevant figures and tables in the article.

Conflicts of Interest

The authors declare that there are no conflicts of interest regarding the publication of this paper.

Acknowledgments

The authors are grateful for the financial support of the research from the National Natural Science Foundation of China (51704101), Key Scientific and Technological Research Projects in Henan Province (182102310780 and 192102310199), and the 65th general program of China

Postdoctoral Science Foundation (2019M6525352536). This work was also supported by the Fundamental Research Funds for the Universities of Henan Province (NSFRF200307).

References

[1] F. Du, K. Wang, X. Zhang, C. Xin, L. Shu, and G. Wang, "Experimental study of coal-gas outburst: insights from coal-rock structure, gas pressure and adsorptivity," *Natural Resources Research*, vol. 29, no. 4, pp. 2481–2493, 2020.

[2] E. Y. Wang, X. Q. He, L. M. Dou et al., "Electromagnetic radiation characteristics and rocks during excavation in coal mine andtheir application," *Chinese Journal of Geophysics*, vol. 48, no. 1, pp. 216–221, 2005.

[3] Y. L. Tan, H. Zhou, X. J. Han et al., "Analysis on acousticemission pattern for rock burst," *Chinese Journal of Rock MeChanics and Engineering*, vol. 19, no. 4, pp. 425–428, 2000.

[4] Y. X. Xia, J. F. Pan, Y. J. Wang et al., "Research on fracture and stress distribution characteristics of coal based on high-precision microseismic monitoring," *Journal of China Coal Society*, vol. 36, no. 02, pp. 239–243, 2011.

[5] N. Li, E. Y. Wang, and M. C. Ge, "Microseismic monitoring technique and its applications at coal mines: present status and future prospects," *Journal of China Coal Society*, vol. 42, no. S1, pp. 83–96, 2017.

[6] N. Li, B. L. Li, and D. Chen, "Multi-fractaland time-varying response characteristics of microseismic waves during the rockburst process," *Journal of China University of Mining & Technology*, vol. 46, no. 5, pp. 1007–1013, 2017.

[7] W. J. Lei, J. Y. Li, and M. H. Yun, "Research on propagation and attenuation characteristics of mining micro-seismic wave," *Rock and Soil Mechanics*, vol. 40, no. 4, pp. 1491–1497, 2019.

[8] W. J. Lei, Z. F. Wang, and Z. Z. Han, "Micro-Seismic characteristics due to mining effects [J]," *Chinese Journal of Rock Mechanics and Engineering*, vol. 34, no. 4, pp. 795–803, 2015.

[9] Q. J. Zhu, F. X. Jiang, Z. X. Yu et al., "Study on energy distribution characters about blasting vibration and rock fracture microseismic signal," *Chinese Journal of Rock Mechanics and Engineering*, vol. 31, no. 4, pp. 723–730, 2012.

[10] F. X. Jiang, Y. M. Yin, Q. J. Zhu et al., "Feature extraction and classification of mining microseismic waveforms via multi-channels analysis," *Journal of China Coal Society*, vol. 39, no. 2, pp. 229–237, 2014.

[11] X. Q. He, A. H. Wang, and L. M. Dou, "Technology of microseismic dynamic monitoring on coal and gas outburst-prone zone," *Journal of China Coal Society*, vol. 43, no. 11, pp. 3122–3129, 2018.

[12] Q. J. Zhu, Q. S. Li, E. H. Zhang et al., "Study on microseismic characteristics of geologic anomaly region in coal and gas outburst seam induced by roadway excavation," *Coal Science and Technology*, vol. 47, no. 7, pp. 39–46, 2019.

[13] Y. Z. Wang and D. Y. Gong, "Study on the microseismic signal characteristics and energy change in the coal mine working face," *China Mining Magazine*, vol. 29, no. S1, pp. 209–212, 2020, dio:.

[14] B. X. Jia, K. Wang, A. Sun, L. L. Zhou, C. Sun, and L. J. Su, "Experimental study on propagation law of microseismic signal in layered rock mass containing goaf [J/OL]," *Rock and Soil Mechanics*, no. 10, pp. 1–11, 2020.

[15] L. H. Kong, F. X. Jiang, S. H. Yang et al., "Movement of roof strata in extra-thick coal seams in top-coal caving mining based on a high precision micro-seismic monitoring system," *Chinese Journal of Engineering*, vol. 32, no. 5, pp. 552–558, 2010.

[16] X. Q. Guo, L. M. Dou, C. P. Lu, Z. K. Li, B. Liu, and C. G. Lu, "Research on the microseismic activity of fault reaction induced by coal mining," *Safety in Coal Mines*, vol. 42, no. 1, pp. 26–30, 2011.

[17] Z. Yang, H.-M. Wang, D.-Q. Sun, X.-J. Ma, M.-B. Xu, and N.-X. Si, "Study on occurrence mechanism of coal pillar in L-shaped zone during fully mechanized mining period and prevention technology," *Shock and Vibration*, vol. 2021, Article ID 6638009, 15 pages, 2021.

[18] J. Ren, W. Zhang, Z. Wu, J. Li, and Y. Shen, "Microseismic signals in heading face of tengdong coal mine and their application for rock burst monitoring," *Shock and Vibration*, vol. 2021, Article ID 6650446, 13 pages, 2021.

[19] W. Yang, X. Li, S. Xie, and S. Ning, "Research on the mechanism and prevention for rock burst of soft coal in deep mine," *Geotechnical and Geological Engineering*, vol. 39, no. 4, pp. 2915–2926, 2021.

[20] S. Wang, G. Zhu, K. Zhang, and L. Yang, "Study on characteristics of mining earthquake in multicoal seam mining under thick and hard strata in high position," *Shock and Vibration*, vol. 2021, Article ID 6675089, 17 pages, 2021.

[21] R. Hardy, *Acoustic Emission/Microseismic Activity*, Vol. 1, A. A. Balkema Publishers, Lisse,Netherlands, 2003.

[22] M. Ge, "Efficient mine microseismic monitoring," *International Journal of Coal Geology*, vol. 64, no. 8, pp. 44–56, 2005.

[23] D. Song, X. He, L. Dou et al., "Research on MS regional detection technology for coal and gas outburst hazard," *China Safety Science Journal*, vol. 31, no. 1, pp. 89–94, 2021.

[24] Z. Li, *Study on Mechanism of Coal Rock Impact Induced by Fault Slip under the Influence of Mining*, China University of Mining and Technology, Xuzhao, China, 2009.

[25] F. Du and K. Wang, "Unstable failure of gas-bearing coal-rock combination bodies: insights from physical experiments and numerical simulations," *Process Safety and Environmental Protection*, vol. 129, pp. 264–279, 2019.

[26] J. Y. Li, W. J. Lei, H. B. Zhao et al., "Micro-seismic characteristics during impact failure of coal and rock under repetitive blast mining," *Journal of China University of Mining & Technology*, vol. 9, no. 5, p. 48, 2019.